Characterization of fresh PM deposits on calcareous stone surfaces: seasonality, source apportionment and soiling potential

Monika Ogrizek[a,b], Asta Gregorič[c,d], Matic Ivančič[c], Daniele Contini[e], Urša Skube[a], Kristijan Vidović[a,f], Marjan Bele[g], Martin Šala[a], Marta Klanjšek Gunde[g], Martin Rigler[c], Eva Menart[h,i], Ana Kroflič[a,j,*]

[a]Department of Analytical Chemistry, National Institute of Chemistry, Hajdrihova 19, 1000 Ljubljana, Slovenia

[b]Jožef Stefan International Postgraduate School, Jamova cesta 39, 1000 Ljubljana, Slovenia

[c]Aerosol d.o.o., Kamniška ulica 39a, 1000 Ljubljana, Slovenia

[d]Center for Atmospheric Research, University of Nova Gorica, Vipavska 11c, 5270 Ajdovščina, Slovenia

[e]Institute of Atmospheric Sciences and Climate (ISAC-CNR), Division of Lecce, Str. Prv. Lecce-Monteroni km 1.2, 73100, Lecce, Italy

[f]Laboratory for Physical Chemistry of Aquatic Systems, Ruđer Bošković Institute, Bijenička cesta 54, 10000 Zagreb, Croatia

[g]Department of Materials Chemistry, National Institute of Chemistry, Hajdrihova 19, 1000 Ljubljana, Slovenia

[h]National Museum of Slovenia, Muzejska ulica 1, 1000 Ljubljana, Slovenia

[i]Jožef Stefan Institute, Jamova 30, 1000 Ljubljana, Slovenia

[j]now at: Department of Catalysis and Chemical Reaction Engineering, National Institute of Chemistry, Hajdrihova 19, 1000 Ljubljana, Slovenia

ABSTRACT

Particulate matter (PM) pollution is one of the major threats to cultural heritage outdoors. It has been recently implied that organic aerosols will prevail over inorganic carbon particulates in the future, changing the main mechanisms of damage caused by poor air quality to calcareous heritage in particular. We studied fresh particulate deposits on marble and limestone surfaces exposed to urban air in sheltered and unsheltered configurations. Due to different air pollution sources in different seasons, the amount and composition of surface deposits varied throughout the year. The main and most constant contributor to $PM_{2.5}$ (particles smaller than 2.5 µm) were primary traffic emissions (30 %), followed by secondary formation of acidic inorganic aerosols, such as sulphate in summer and nitrate in winter (33 % altogether), and seasonal biomass-burning emissions (14 %). Although biomass burning is the major source of primary organic aerosols including the light-absorbing fraction that prevailed over black carbon (BC) in colder months (upto 60 % carbonaceous aerosol mass), we show that surface darkening causing the soiling effect is still governed by the minor BC fraction of atmospheric aerosols, which remained below 20 % of the carbonaceous aerosol mass throughout the year. This, however, can change in remote environments affected by biomass-burning emissions, such as winter resorts, or by rigorous BC mitigation measures in the future. In the short run, sheltered positions were less affected by different removal processes, but we show that surface deposits are not simply additive when considering longer periods of time. This must be taken into account when extrapolating surface accumulation to longer time scales.

1 Introduction

Outdoor materials are permanently exposed to weathering in combination with air pollution. Their interactions with airborne pollutants lead to material degradation (atmospheric corrosion) and loss, including deterioration of cultural heritage objects causing immeasurable damage to the community (Tidblad et al., 2012). Surface blackening due to particulate matter (PM) deposition (soiling) is another major hazard to heritage materials (Lombardo et al., 2010), requiring periodical cleaning and often resulting in unwanted damage especially to stone objects (Brimblecombe and Grossi, 2005).

In the past century, SO_2 was by far the most important factor influencing calcareous stone recession outdoors (Giavarini et al., 2008). Until now, SO_2 emissions have been successfully mitigated and the situation has changed from SO_2-dominant to a multipollutant one (Vidović et al., 2022). Recently, comparable contributions of dry HNO_3 deposition (closely connected with NO_x emissions and O_3 in combination with moisture), SO_2 deposition, acidic precipitation (due to dissolved CO_2 (Karst effect) and anthropogenic H_2SO_4 and HNO_3 acids in acid rain), and PM deposition to limestone deterioration have been estimated in urban areas (Bonazza et al., 2009; De Marco et al., 2017). However, according to Di Turo et al. (2016), increased PM concentrations were responsible for the estimated positive trend in limestone corrosion levels between years 2000 and 2010 in Europe, which warrants attention.

Airborne PM, which affects stone surfaces with both soiling and surface corrosion, is typically composed of inorganic ions, trace metals, and carbonaceous aerosol (CA), which includes two fractions: black carbon (BC or elemental carbon) and organic aerosol (OA) that can be further divided into the light-absorbing OA or brown carbon (BrC) and non-absorbing OA ($OA_{non-abs}$). Carbon content in CA and OA is often expressed as total carbon (TC) and organic carbon (OC), respectively. The composition of PM is closely linked to its emission sources, thus exhibiting strong seasonality. For instance, BC originates from various combustion sources (vehicle emissions, residential coal and biomass burning emissions), contributing at varying amounts to

4

the level of BC pollution throughout the year, while biomass burning specifically is recognized as the major source of BrC on a global scale (Laskin et al., 2015), which is consequently predominant in colder months due to wide use of fireplaces and wood burning for heating. On the other hand, $OA_{non-abs}$ is largely connected with biogenic emissions and predominates in remote regions and in the warmer part of a year (Martinsson et al., 2020).

The reactive OA fraction has been found to predominate over the more inert BC in black crusts of historic buildings at many sites in Italy, which contradicts the general belief that BC is responsible for damage caused to calcareous historic objects (Bonazza et al., 2005). Already back in 1993, Saiz-Jimenez (1993) studied deposition of airborne organics on historic buildings and concluded that composition of each crust is governed by the composition of the air in the area. In support, Bonazza et al. (2005) showed that historic damage layers are a record of environmental changes over time, with their chemical composition reflecting atmospheric pollution due to combustion sources, and concluded that soiling due to OA will likely prevail in the next future. Akos et al. (2011) further compared the content of polyaromatic hydrocarbons (PAH) in ambient PM and in the crusts of historic buildings, and recognized the important role of dust in accumulating PAHs. Moreover, Ozga et al. (2014) concluded that damage layer composition reflects air pollution in the surrounding area; however, Fermo et al. (2018) did not find any direct correlation between atmospheric gaseous precursors and the related ions in investigated PMdeposits.

While the exact role of atmospheric PM in stone degradation remains elusive (Fermo et al., 2015), it is clear that surface deposits can contain atmospheric particles from both natural and anthropogenic sources (Calparsoro et al., 2017). Although BC is unequivocally recognized as the major contributor to surface soiling, very little to nothing is known about the influence of the increasing BrC fraction in atmospheric aerosols and how unique physico-chemical characteristics of ambient PM from different sources in different seasons affect particulate deposition and stone surface degradation beyond the damaging potential of contained inorganic acids.

In this work, we analyse fresh seasonal PM deposits on calcareous (limestone and marble) stones representing the majority of cultural heritage objects, in order to later compare them with aged stone surfaces. We first physico-chemically characterize atmospheric PM in Ljubljana, Slovenia in order to correlate surface properties of exposed carbonaceous stones with different PM pollution conditions in different seasons. During one-month outdoor exposures of stones under sheltered and unsheltered conditions, ambient $PM_{2.5}$ samples (*i.e.* airborne particulatessmaller than 2.5 µm) were collected and analysed for ionic and elemental composition. In parallel, PM size distribution, TC concentration and optical properties were measured and used to apportion carbonaceous aerosols to their sources (traffic, biomass burning; primary, secondary aerosols) and particular light-absorbing fractions (BC, BrC, $OA_{non-abs}$). Positive matrix factorization (PMF) analysis was further applied to identify the main sources of PM pollution atthe site of exposure, which differ with different seasons. Specific methodology was set up for stone surface characterization after each exposure; stones were investigated for their surface morphology, reflectance (as a measure of soiling), and elemental composition, which is finally correlated with airborne $PM_{2.5}$ measurements.

2   Experimental section

2.1   *Location and experimental design*

Surface-polished limestone and marble samples (5×5×1.5 cm; **Figure 1**a) were exposed to outdoor weathering and urban pollution on the terrace of the National Institute of Chemistry in Ljubljana, Slovenia. The stones were vertically mounted on a custom-made carousel, in sheltered and unsheltered positions (**Figure 1**b-d). One-month seasonal exposures were performed fromJuly 2020 to July 2021. One limestone and one marble stone were exposed in every position in each season (autumn: 3.11.–4.12.2020; winter: 19.1.–17.2.2021; spring: 14.5.–18.6.2021; summer: 26.6.–26.7.2021), while one set of stones (2+2) was periodically exposed in all four consecutive seasonal campaigns (*i.e.* 14.7.–19.8.2020, 3.11.–4.12.2020, 19.1.–17.2.2021, 14.5.–

18.6.2021). After each exposure, stones were analysed for surface reflection and stored in a freezer until further analyses. During the project, one stone of each type was stored in a laboratory and used as a blank sample for chemical analyses.
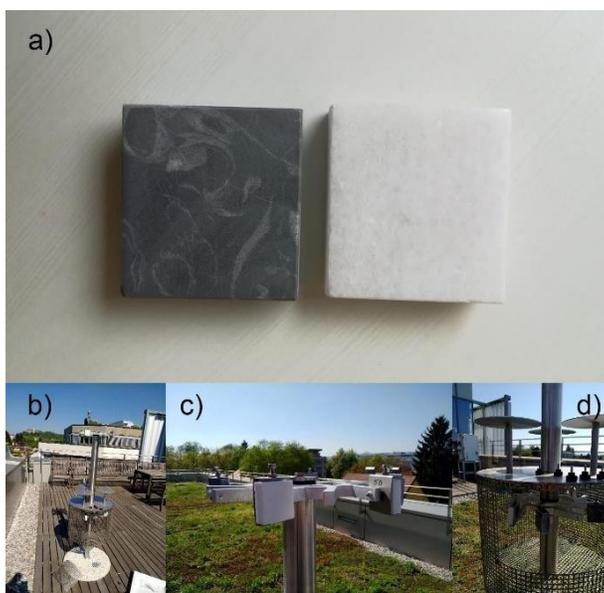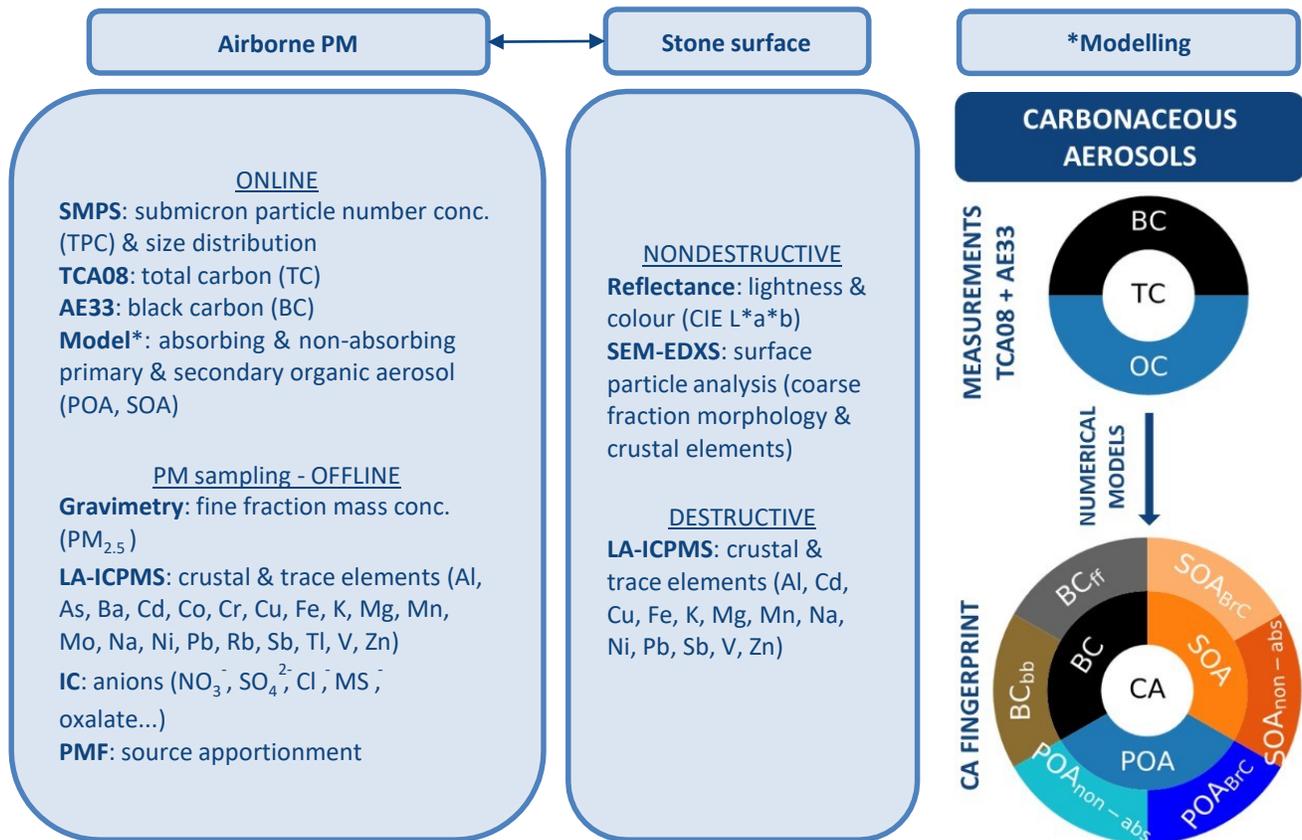

Figure 1: a) Limestone (grey) and marble (white) stone that were exposed on b) custom-made carousel for air pollution exposure studies with c) unsheltered and d) sheltered positions for stone samples.

In parallel, air quality monitoring with an emphasis on atmospheric PM was conducted with dedicated online instrumentation and sampling for offline analyses. At the end, two-weeks data was analysed for every campaign; the list of samples and corresponding meteorological conditions are collected in the Supporting information, **Table S1**.

2.2   Materials and methods

Performed analyses and selected measurement parameters are schematically presented in **Scheme 1**.

Scheme 1: Schematic representation of the experimental design including the flow chart of eight steps modelling procedure to apportion carbonaceous aerosol into six components.

During the campaigns, particle number concentration and number size distribution were measured in real time using a Scanning Mobility Particle Sizer (SMPS Spectrometer 3936L75, TSI). Measurements of TC and BC were performed with a Carbonaceous Aerosol Speciation System (CASS, Magee Scientific), which is a combined unit of a TCA08 Total Carbon Analyzer (Rigler et al., 2020) and the Aethalometer® AE33 (Drinovec et al., 2015). TCA08 measures the concentration of TC by a rapid combustion of PM collected on a quartz filter at 940 °C and was operated at 1-hour time intervals, sampling $PM_{2.5}$ fraction at $16.7 \, \mathrm{L \, min^{-1}}$. The tandem Aethalometer AE33 measures aerosol light absorption at seven wavelengths (370 nm, 470 nm, 520 nm, 590 nm, 660 nm, 880 nm and 950 nm) and reports equivalent BC concentration at 880 nm by applying a specific mass absorption cross-section (7.77 $\mathrm{m^2/g}$). Again, a size-selective inlet was used to sample $PM_{2.5}$ at a flow rate of $5 \, \mathrm{L \, min^{-1}}$. High time-resolution data (1 minute resolution) was then averaged to 1 hour, to synchronize with the TC measurements. AE33 uses a

"dual-spot" methodology to correct for the filter loading effect in real-time (Drinovec et al., 2015). The multiple scattering in the filter matrix was corrected by a correction factor C of 1.39. The difference between TC and BC corresponds to the OC fraction (Rigler et al., 2020). Online BC, TC and OC concentrations were later validated by comparison with offline analysis of PM samples (**Figure S1**).

Atmospheric PM samples were simultaneously collected on quartz fibre filters (Pall Tissuquartz™ 2500 QAT-UP, Φ47 mm) using a low-volume PM sampler (Giano, Dado lab) with a $PM_{2.5}$ impactor head. Air flowrate was 2.3 m^3 h^{-1} and after 24 h sampling, filters were stored in a cooled compartment inside the sampler. The filters were conditioned in a thermostated room for at least 24 h prior to weighing before and after sampling (22±1 ˚C, 50±5 % RH), and average daily $PM_{2.5}$ concentrations in the air were calculated. However, quartz fibre filters are very fragile and quite some masses obtained were negative. Therefore, $PM_{2.5}$ concentrations as obtained from the nearest air quality monitoring station of the Slovenian Environment Agency (ARSO, approx. 5 air km distance) are considered in this work (**Table S1**). When available, our $PM_{2.5}$ concentrations correlated well with the data obtained from ARSO (**Figure S2**). Every filter was cut in pieces needed for particular analysis and kept in a freezer.

As is typical for ion analysis, the anions were determined and quantified with ion chromatography. One cm^2 filter was extracted in 1 ml MilliQ water (18.2 mΩ cm at 25 °C, <3 ppb TOC) on an orbital shaker at 300 rpm for 30 min. MilliQ water was daily collected fresh from a Millipore purification system (Bedford, MA, USA). Extracts were filtered (RC, 0.20 μm) and analysed with a Dionex ICS 3000 chromatograph equipped with an eluent generator and a conductivity detector. A precolumn (Dionex IonPac AG11-HC, 4×50 mm) and an analyticalcolumn (Dionex IonPac AS11-HC, 4×250 mm) were used to achieve desired analyte separation. More details about the analysis are given in Kušan et al. (2020). The following anions were successfully quantified in the samples: fluoride, lactate, methanesulfonate (MS), chloride, nitrite,

nitrate, sulphate, oxalate, and phosphate. Their measured airborne concentrations can be found in

Table S2. Although cations are also typically measured by ion chromatography, Na, K, Ca and Mg were rather determined together with other trace elements by laser ablation inductively- coupled plasma mass spectrometer (LA-ICPMS, see below).

Elemental composition of collected PM was determined directly from a solid sample by a nanosecond excimer laser ablation (LA) system (193 nm ArF*; Analyte G2, Teledyne Photon Machines Inc., Bozeman, MT) interfaced with a quadrupole inductively-coupled plasma mass spectrometer (ICPMS; Agilent 7900x, Agilent Technologies, Santa Clara CA). The method is described in detail elsewhere (Ogrizek et al., 2021) and it has been shown to be competitive with other elemental analysis techniques in the case of PM (Ogrizek et al., 2022) as well as heritage materials (Giussani et al., 2009). Briefly, the filter samples were cut and simply mounted on a microscopic glass and inserted into a holder for analysis. The ablation was performed in a HelEx II two-volume ablation cell with helium as a carrier gas (cup flow 0.5 L min^{-1} and cell flow 0.3 L min^{-1}) and argon as a makeup gas (0.8 L min^{-1}). NIST glass SRM 612 was measured before and after every sample to observe potential instrument drift during the several-hour measurement. Instrument operation parameters are shown in **Table S3**. Every time, 3×12 mm^2 of a PM loaded filter was ablated, which has been shown representative of the whole filter (Ogrizek et al., 2021). Calibration was performed by measuring matrix-matched standards under the same operation conditions on the same day. Since a suitable matrix-matched reference material is not commercially available, PM$_{10}$ samples collected on quartz fibre filters in different seasons in Maribor, Slovenia, for which elemental concentrations had already been determined with a standard method by microwave digestion and ICPMS according to EN14902, were used forcalibration purpose. Twenty elements (Al, As, Ba, Cd, Co, Cr, Cu, Fe, K, Mg, Mn, Mo, Na, Ni,Pb, Rb, Sb, Tl, V, and Zn) were measured simultaneously and the corresponding airborne concentrations are given in **Table S4**.

At the end of every campaign, stones were analysed for their surface deposits and reflectance. Scanning electron microscopy (SEM) and energy dispersive X-ray spectroscopy (SEM-EDXS) were carried out using an FE-SEM Zeiss Supra TM 35 VP (Carl Zeiss, Oberkochen, Germany) field emission scanning electron microscope equipped with an energy-dispersive X-ray (EDX) spectrometer SDD EDX Ultim Max 100 (Oxford Instru-ments, Oxford, UK). The operating voltage was set to 1 kV for SEM and 20 kV for EDXS. Reflectance of the samples were measured using an i1-Pro spectrometer (X-Rite) in the visible spectral range (380–730 nm in 10-nm steps) with 45°/0° ring illumination optics (DIN 5033). The diameter of the measurement aperture is 4.5 mm. Each measurement was performed on 3 identical-location sampling positions and average values are reported for every sample.

Elemental composition of the deposits was studied with the same LA-ICPMS system as used for the PM samples, with use of similar instrumental parameters. The only difference was the lower fluence used in this case (0.43 J cm^{-2}), because the goal was to ablate only the deposited PM material without the stone itself. Note that a high background signal from the stone could hinder the analysis or even cover up the signal of trace elements present in the deposited PM. Moreover, fewer elements (Al, Cd, Cu, Fe, K, Mg, Mn, Na, Ni, Pb, Sb, V, and Zn) were measured on the stone surfaces, so that the sensitivity was improved by prolonging the dwell times used. The ablation set-up for each stone consisted of 5 separate lines of 3 cm in length, with the starting position 1 cm from each edge (**Figure S3**).

2.3   Statistical analysis

Apportionment of different carbonaceous aerosol components to their sources relies on a specific information available in the measured dataset. The concentration of OC was derived from a difference between the TC and BC concentrations. Moreover, spectrally resolved optical absorption measurements differentiate between different BC sources (from traffic – BC_{ff} and from biomass burning – BC_{bb}), and between BC and BrC absorption. The EC (BC) tracer model was used to split OC into primary (POC) and secondary (SOC). Similarly, the modified BC tracer

11

model was used to further split between primary (POA_{BrC}) and secondary BrC (SOA_{BrC}), where different values of mass absorption coefficient (MAC) were used to calculate the eqivalent mass of primary and secondary BrC ($MAC_{BrC,prim}$ = 5.5m^2/g and $MAC_{BrC,sec}$ = 2.4 m^2/g). A constant, season-independent factors of POA/POC = 1.2 and SOA/SOC = 1.8 were applied to convert the carbon mass into the aerosol mass. In the last step, aerosol mass concentration of non-light-absorbing aerosols was estimated using a mass closure ($POA = POA_{non-abs} + POA_{BrC}$ for primary organic aerosols and $SOA = SOA_{non-abs} + SOA_{BrC}$ for secondary organic aerosols, respectively). Workflow is presented in **Scheme 1** and detailed methodology in the work of Ivančič et al. (.

Source apportionment of $PM_{2.5}$ was performed using a PMF receptor model applied with the EPA-PMF5 software. The EPA PMF5 software has been widely applied to the characterisation of PM sources (Belis et al., 2020; Cesari et al., 2016). It is based on a multi-linear engine (ME) that allows for the application of specific constraints to PMF outputs (Paatero et al., 2014). The dataset used as an input included particulate ions, elements, OC, BC_{ff}, and BC_{bb}. Considering the Signal-to-Noise (S/N) criteria and the number of data above the detection limit, input variables of fluoride, lactate, and nitrite were classified as "bad" and were not included in the PMF analysis. All the other variables were classified as "strong". This resulted in a dataset of 69 samples with 26 chemical species as input parameters including $PM_{2.5}$ used as the total variable. Different runs were carried out with different number of factors and the best solution was obtained with six factors representing six different sources. PMF5 was applied using specific constraints on factor profiles in order to limit rotational ambiguity and obtain more interpretable source profiles. Specifically, in the road traffic factor/source constraints were applied to BC_{ff} (pull up maximally) and BC_{bb} (pull down maximally). The expectation value (Q) of each constraint was within 1 % and the final Q-value obtained with respect to the base run was 0.5 %. The uncertainties on the profiles and the contributions of the different factors were evaluated using the bootstrap method (Paatero et al., 2014) in terms of one standard deviation.

Images resulting from the 2D elemental analysis of PM filters with LA-ICPMS were processed as described in Ogrizek et al. (2021). For the intercomparison between different campaigns, elemental and ionic composition results were analysed as described for stone samples. For the analysis of stone surface deposits, background signal was first subtracted from gas blank and outlier pixels were removed (the rule of three interquartile ranges was applied, same as for PM samples; see Ogrizek et al. (2021)). An average of every line was considered one unit in this case. Elemental composition results were compared as follows: (i) every exposure stone was compared with a blank stone sample, (ii) for every campaign, sheltered and unsheltered treatments were compared, and (iii) different campaigns were compared with each other. For the basic overview over the working dataset, the Shapiro-Wilk test was performed, as well as the Q-Q plot for assessing the normality and Levene's test for testing the equality of variances. Since the majorityof data was not normally distributed and/or did not exhibit equal variances, a non-parametrical statistical test was selected for statistical evaluation. Mann-Whitney test was used to investigate differences between two sample groups (*i.e.* to compare every sample with a blank or compare sheltered to unsheltered samples). The comparison of seasonal campaigns (*i.e.* to obtain differences between multiple groups) was made with use of the Kruskal-Wallis and Dunn's post hoc test. Benjamini & Hochberg p-value adjustment method was applied in all multiple comparisons. Statistical analysis was performed using program R with raster, data.table, reshape2 (Wickham, 2007), tidyverse (Wickham et al., 2019), rstatix, and ggpubr packages.

3   Results and discussion

3.1   *Characterization and source apportionment of atmospheric aerosols in different seasons*

Atmospheric total particle number concentration (TPC) in the size range of 14–750 nm, TC and BC were measured in near-real time. Typical diurnal profiles (**Figure S4**) exhibit bimodal shape peaking in the morning and at night, which is associated with the dynamics of the atmospheric mixed layer and diurnal emission patterns (*e.g.*, rush-hour) (Manning et al., 2018). Bimodality is

especially pronounced in winter, which can be attributed to morning temperature inversion common for the Ljubljana basin. During temperature inversion, the height of the mixing layer is substantially reduced and concentrations of primary pollutants that are trapped within this relatively narrow layer of air consequently increase. Note that in February 2021 there was a lotof sun, which is needed for this meteorological phenomenon.

Time series of TPC, TC and BC are shown in **Figure S4**. Except for some momentary BC spikes, fair agreement is observed between the three parameters in all seasons. This can beattributed to predominant traffic emissions as a constant pollution source in the city. As regardsthe spikes, careful examination of the corresponding contour plots revealed a sudden income of relatively large carbonaceous aerosols, *i.e.* bigger than the diameter at which total number concentrations peaked (*i.e.* at 60-100 nm). These particles did not contribute much to the total number concentration, while they increased particle mass significantly, which is thus only observed in the TC and BC parts of the time series. In general, much higher TPC, TC and BC concentrations are characteristic of cold seasons compared to the warmer months (by roughly a factor of two).

Airborne concentrations of selected elements in all five seasonal campaigns are presented and compared in **Figure S5**. For K, Mg, Na, and Tl quantification was not possible; therefore, their relative contributions as measured by LA-ICPMS are additionally shown in **Figure S6**. Based on the obtained seasonal pattern, a quick inspection divides the elements into two groups: i) those enriched in colder months (autumn and winter; *e.g.* As, Cd, Cr, Mn, Mo, Pb, Rb, Zn) are characteristic of fossil-fuel combustion emissions, whereas ii) those with higher concentrations and scattering observed in February and June 2021 (*e.g.* Al, As, Co, Fe, Mn, Rb, V, also K, Mg, Na, Tl) can be attributed to Saharan dust events that were reported in the respective periods of time (23.–26.2.2021 and 21.–24.6.2021).

Characteristic seasonal patterns were also observed for chloride, nitrate, and methanesulfonate (**Figure S7**). Nitrate and chloride concentrations peak in autumn and winter, which can be

attributed to wood combustion for heating purposes. Methanesulfonic acid, on the other hand, is one of the most important secondary organic aerosol components in marine environments. It isthe oxidation product of gaseous dimethylsulfide that is emitted from the ocean due to phytoplankton activity especially in warmer months (Mansour et al., 2020). Methanesulfonate was indeed predominant in PM collected in the spring and summer campaigns.
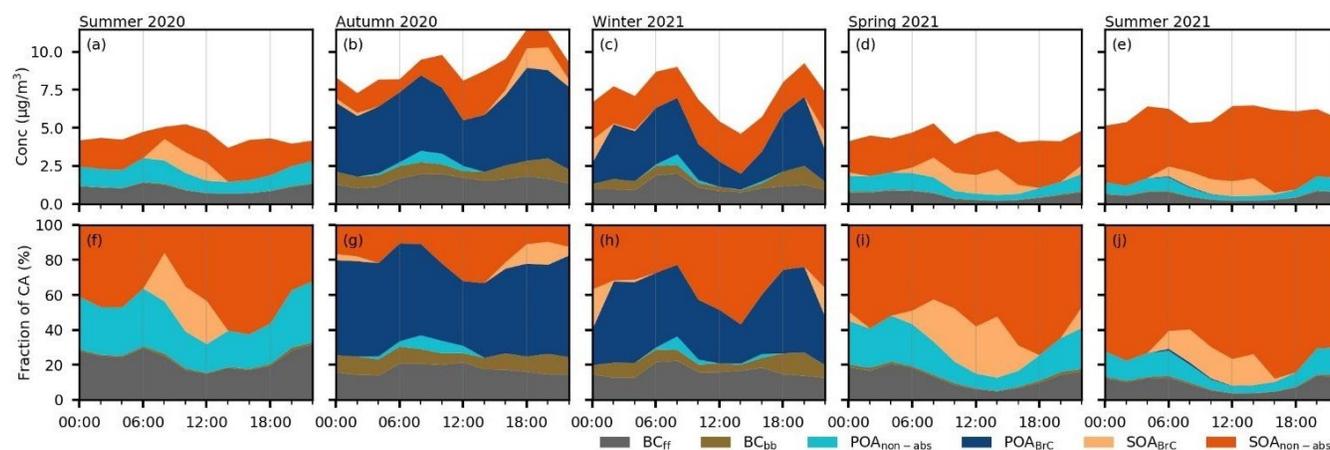

Figure 2: Apportionment of carbonaceous aerosols to different sources in five seasonal campaigns (summer – August 2020; autumn – November 2020; winter – February 2021; spring
– May-June 2021; summer – June-July 2021); black carbon from traffic (BC_{ff}) and biomass burning (BC_{bb}), non-absorbing and absorbing primary organic aerosols ($POA_{non-abs}$ and POA_{BrC}), and non-absorbing and absorbing secondary organic aerosols ($SOA_{non-abs}$ and SOA_{BrC}).

Carbonaceous aerosol source apportionment plots are shown in **Figure 2**. In autumn and winter, biomass-burning emissions contributed substantially (BC_{bb} and absorbing primary organic aerosols – POA_{BrC}), while the contribution of SOA was minor in this time of the year. In summer, SOA represents more than half of the total carbonaceous aerosol mass, which is due to pronounced photochemistry, while BrC aerosols only contribute a small portion of it, during daytime. Non-absorbing aerosols ($POA_{non-abs}$+$SOA_{non-abs}$) represent roughly 60–80 % of the carbonaceous aerosol mass in summer. Although we conducted a campaign already in very late spring, there is still some evidence of biomass-burning emissions, probably due to agricultural waste burning. The contribution of non-absorbing aerosols in spring was similar to the summer periods. Traffic emissions tend to be relatively constant throughout the year and stabilized

somewhere below 20 % of the carbonaceous aerosol mass. It should be noted at this point that especially autumn and winter campaigns were affected by restrictions due to the coronavirus pandemic, which could result in lower-than-usual traffic emissions in these seasons (only slightly higher absolute BC_{ff} concentrations were determined in the cold seasons compared to the warmer months).
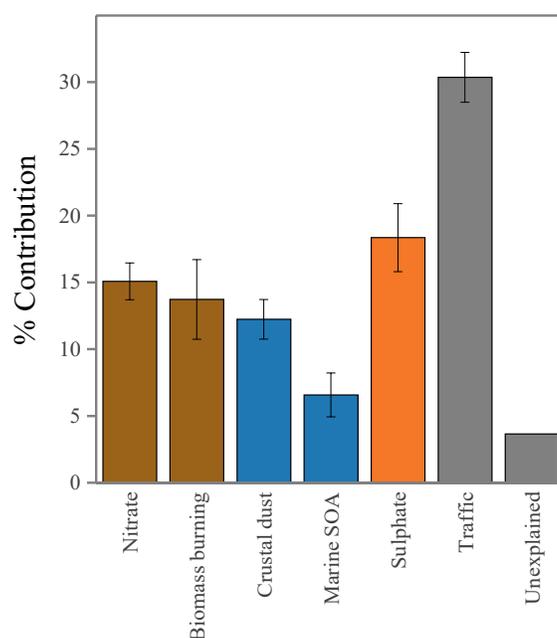

Figure 3: Relative contribution of sources to the investigated PM; six PMF factors are identified, unexplained refers to the fraction of $PM_{2.5}$ which could not be reconstructed by the PMF model (~4 %). Typical winter sources are coloured brown, summer orange, in blue are special events that can potentially occur at any time of the year and in grey we represent sources that were rather constant throughout the year.

Combining elemental and ionic composition (airborne concentrations are reported in **Table S2** and **Table S4**), OC and BC content, PMF analysis was further performed and confirmed traffic as the main PM pollution source in Ljubljana, Slovenia, contributing with 30 % to the investigated $PM_{2.5}$ mass. Similar has been observed by Saraga et al. (2021). The other factors, which together with traffic accounted for roughly 96 % of the analysed PM, are: secondary inorganic aerosols (nitrate (15 %) and sulphate (18 %)), biomass burning (14 %), mineral dust (12 %), and marine-

rich biogenic SOA (7 %). Relative source contributions are given in **Figure 3**, while the profiles of the different factors are reported in **Figure S8**.

Nitrate (factor 1) and sulphate (factor 4), as indicators of inorganic secondary atmospheric aerosols that may have travelled long distances, are characteristic of different seasons, *i.e.* winter and summer, respectively. While sulphate is typically linked with photochemistry and thus accompanied with SOA (*e.g.* oxalate), winter nitrate can be attributed to combustion emissionsdue to heating purposes (including biomass burning). Correspondingly, biomass burning factor 2 (BC_{bb}, phosphate, chloride, Cd, Pb, OC etc.) predominates in colder months (domestic heating), whereas isolated events can also be identified in other periods of time (agricultural activities, eventually natural fires). Factor 6 represents a contribution related to biogenic SOA, strongly enriched with methanesulfonate and accompanied with sulphate and oxalate. Therefore, this factor is indicated as biogenic SOA likely of marine origin as also found in other areas (Srivastava et al., 2019). Three special events characterized by huge amounts of crustal elements (Al, As, Ba, Co, Cr, Fe, Mn, Rb, V) are described with factor 3, which were confirmed with the advection of Saharan dust in the region. The most constant PM emission source throughout the year is traffic (factor 5), which is especially enriched with metals, such as Ba, Co, Cu, Fe, Mo, Ni, Sb, V, Zn, and BC_{ff}.

3.2   Correlation between air pollution and stone surface deposits

Stone surfaces were analysed for their elemental composition in a similar way as $PM_{2.5}$ on the filters. Although we optimized LA-ICPMS measurement conditions for the sole ablation of PM deposits, ablation of the underlying stone could not be completely avoided. Therefore, we first compare the exposed samples with their (clean) blanks. In **Figure S9** we can see that the amount of Cd on the exposed stones is not statistically different from the blanks. Moreover, crustal elements in the stone matrix (such as Mg, Mn and Na) hindered their accurate quantification inPM deposits. Lower amounts of these elements were sometimes measured in the exposed samples

compared to blanks, which could result from the surface erosion due to weathering and soluble minerals dissolution, but also from the measurement error because of high blank signals.

Although surface analysis was difficult due to trace concentrations and besides, removal processes also influence deposits, a general agreement was found between airborne $PM_{2.5}$ concentrations and PM deposits on the stones. One such example is shown in **Figure 4** for Zn and Al on the sheltered marble samples. Zinc is connected with fossil-fuel combustion, and is thus a typical winter pollutant, which is evident from both, $PM_{2.5}$ and deposit measurements. On the other hand, Al is one of the crustal elements and was thus especially enriched during the Saharan dust events. It should be noted, however, that coarse particles (*i.e.* those bigger than 2.5 µm) also influenced surface deposits compared to the filter results, which is discussed below. Moreover, the winter measurement campaign was a bit delayed with respect to the stone exposure, for which reason the mineral dust storm only affected PM filter results and not stone surface deposits. This is nicely seen in the dataset.
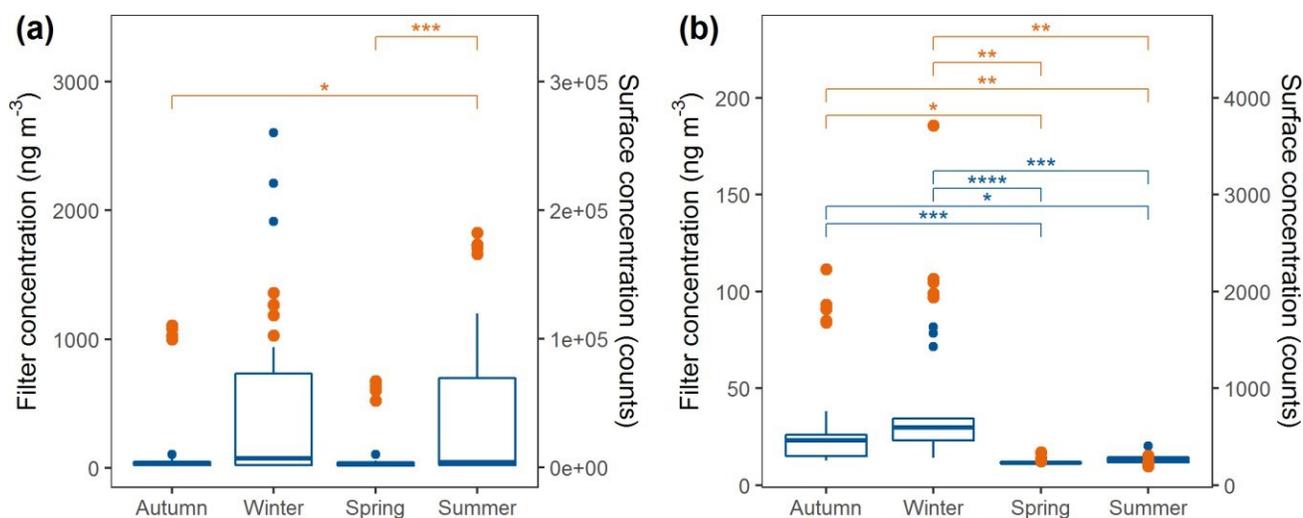

Figure 4: Airborne (blue) vs. surface deposit (orange) concentrations of a) Al and b) Zn in four different seasons (November 2020–July 2021). Winter stones were not subjected to the air masses from Sahara, which influenced concentrations of crustal elements on the filters substantially. Statistically significant differences ($p<0.05$) are marked with asterisk (the more asterisks the more significant the difference).

Although seasonality of the deposits was poorly pronounced and depended on the element, we were able to statistically confirm some differences between the exposed stones (**Figure S10**). Two characteristic features could be identified in the elemental fingerprint of stone surfaces that deserve special attention. Autumn enrichment in Mg, Mn, Na and Pb does not correlate with airborne measurements (except for Pb) and points to the contamination with soil, which indeed usually contributes to the coarse PM fraction and not $PM_{2.5}$. We attribute these observations to gardening on the terrace where passive collectors were installed. The exception is Pb, which can be linked with another PM source, that is road dust resuspension. On the other hand, huge amounts of Al, Fe, K, Mg, Mn, Na and V in summer samples can be linked with the Saharan dust advection, which correlates well also with the measured airborne $PM_{2.5}$ compositions.
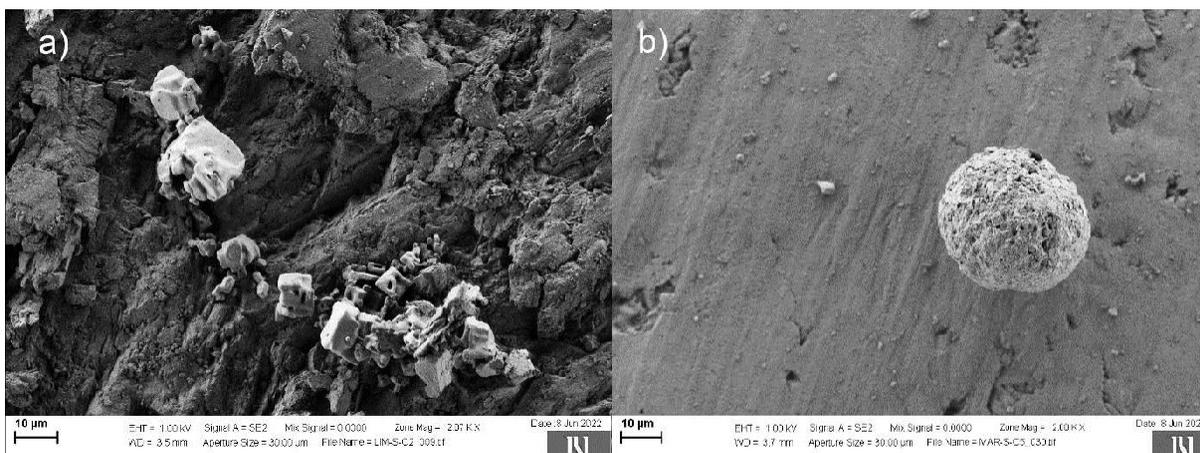

Figure 5: SEM image of a) irregular halite crystals on a sheltered marble (Na, Cl, C) and b) diatomaceous earth/auxospore on a sheltered limestone (Si, Al, Fe, Mg, K).

These elemental analysis results are further supported by microscopy. Especially the sheltered marble stone from the autumn campaign was full of halite crystals (Na, Cl), many of which must have crystalized after PM deposition with the interference of some other (carbonaceous) material that made crystals grow into irregular shapes (**Figure 5**a). On the other hand, on the surface of the sheltered limestone from the summer campaign, a plethora of coarse spherical particles that resembled biological pollen were found (**Figure 5**b). However, their composition (Si, Al, Fe) pointed to the fossilized diatoms or their auxospores, which are typical of desert depressions such

as Bodélé Depression of the Sahara Desert (Assmy et al., 2008; Todd et al., 2007). All of these particles are coarse mode and did not contribute to our airborne $PM_{2.5}$ concentrations, which explains the lack of agreement between PM and surface concentrations for these particular elements. Moreover, large particles are very easily removed and are not expected to contribute to surface deposits in the long run.

When sheltered and unsheltered exposure positions are compared (**Table S5**), less significant differences are found in the case of more heterogeneous limestone samples with more impurities in their original matrix. In general, however, sheltered stones exhibited higher surface concentrations of the measured elements than unsheltered stones exposed concomitantly. This stems from the comparable PM deposition and limited removal processes in the case of sheltered positions, while unsheltered stones were rain-washed at least once during every campaign. Although one sample set was exposed four-times, in all four consecutive campaigns, their elemental content rarely exceeded all the other four seasonal exposures (see **Figure S10**), even in the sheltered position. This points to the importance of diverse removal processes, besides rainfall.

3.3   Surface reflectance measurements

Reflectance measurements were evaluated in the CIELAB colour space in order to distinguish between BC, a typical traffic-related pollutant emitted in the atmosphere throughout the year, and biomass-burning related BrC aerosol impacts peaking in cold seasons. The colour space uses L* for lightness, and a* and b* indicate the four complementary colours of the human vision (red– green and yellow–blue axes, respectively). While BC is known to absorb light in the whole visible range, wavelength-dependent light absorption is characteristic of BrC and increases towards the UV range. Therefore, BrC compounds (as well as BrC particles) are typically yellow-to-brown, which could reflect on a surface they deposit on, if only the surface coverage is sufficient. This may cause changes of a* and b*.

Reflectance data for marble and limestone samples before and after the exposure in four seasonal campaigns in sheltered and unsheltered positions are shown in **Table S6**. First, *L** is

considered as a measure of soiling. In the case of unsheltered white marble stones, significant difference was mostly detected between blank and exposed stones (except in winter). However, surface lightness is increased and not decreased, which cannot be attributed to the deposition of absorbing (BC) particles. Stone whitening was also observed on almost all limestone samples that are originally greyish in colour. As bleaching does not seem to correlate with ambient particle concentrations in different seasons, non-absorbing aerosol deposition is not expected to contribute in these short-term exposures. In fact, stone bleaching is usually attributed to optical effects due to weathering effects, as a consequence of changes in the surface roughness (Marszałek and Skowroński, 2010).

Although BrC concentrations varied much more through the year than the level of BC pollution, no significant colour changes were measured for any of the samples exposed in one-month campaigns that could be correlated with seasonal PM composition.

Besides one-month exposures, one set of stones was also exposed in all four seasonal campaigns (**Table S7**). In this case, initial bleaching followed by a gradual darkening of the surface was observed (except for the sheltered limestone), which could be related to PM deposition (soiling). Again, the colour of marble did not change significantly during the exposure, whereas limestone exhibited more blue tones after all four campaigns (for both, sheltered and unsheltered positions). None of the analysed stones, however, reflected in the yellow-red regions, which are typical of BrC components.

Although we cannot draw conclusions about BrC soiling based on the monthly exposure data, the methodology seems appropriate for long-term exposure studies which are ongoing in the laboratory, as air quality data confirmed predomination of BrC particles over BC in the atmosphere. BrC aerosols accounted for up to 60 % carbonaceous aerosol mass in the colder part of the year (with minor contribution in summer), while BC remained below 20 % in all seasons. However, the bigger PM amount does not necessarily reflect in increased soiling, since optical

characteristics play an equally important role in the cumulative effect as the concentration.
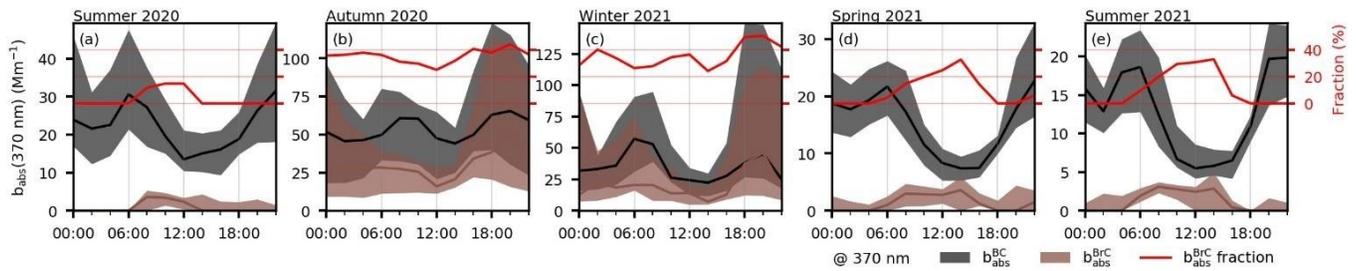
Figure 6: Seasonal diurnal profiles of optical absorption by the measured black carbon (b_{abs}^{BC}) and brown carbon (b_{abs}^{BrC}) at 370 nm: median, Q1 and Q3.

Therefore, in **Figure 6** we further compare optical absorption of measured carbonaceous aerosols by BC and BrC at 370 nm. The data show that BC absorption still exceeds BrC absorption in all seasons and the difference in absorption is expected to be even bigger in the visible range of the spectrum. Nevertheless, with applying BC limits at the national level and more rigorous preventive measures for BC abatement, the situation may change already in the near future.

4   Conclusions

We can conclude that fresh PM deposits on calcareous stone surfaces roughly resemble the composition of airborne PM; the higher the exposure to a particular pollutant, the bigger its amount on the stone surface in the short run. In this sense, more polluted seasons and areas pose a bigger treat to stone heritage objects, especially when it comes to fast corrosion processes. On the other hand, we also show that particulate accumulates do not simply sum up in the long run. Therefore, linear extrapolation from short-term exposures could lead to erroneous prediction results. Although sheltering protects stone surfaces from wet removal processes (*e.g.* rain wash, dew), other removal processes such as surface-wind interaction seem comparably important when considering PM accumulation on a surface.

Due to opposing effects of stone weathering causing optical whitening of the surface and soiling, absorbing aerosol deposition could not be evaluated in the performed 1-month campaigns. Nevertheless, we show that BC absorption exceeded BrC absorption at 370 nm in all seasons, which confirms BC is still a predominant soiling factor in urban sites like Ljubljana, Slovenia.

This, however, can change in less polluted environments and in the future, once BC emissions will be successfully mitigated.

In this study we advance a holistic methodological approach of other groups (*e.g.* Fermo et al. (2015); Winkler et al. (2022)) to studying PM deposition, aging and removal processes on calcareous stone surfaces as well as stone surface degradation with non- and micro-destructive techniques, which can help predict the fate of cultural heritage objects in polluted environments and adopt most suitable mitigation measures.

ACKNOWLEDGMENTS

COMPETING INTERESTS

Asta Gregorič, Matic Ivančič and Martin Rigler are employed by the company Aerosol d.o.o., which develops and manufactures aerosol instrumentation, including the CASS instrument usedin the campaigns.

REFERENCES

Akos T, Licha T, Simon K, Siegesmund S. Urban and rural limestone weathering; the contribution of dust to black crust formation. Environmental Earth Sciences 2011; 63: 675-693.

Assmy P, Hernandez-Becerril DU, Montresor M. Morphological variability and life cycle traits of the type species of the diatom genus Chaetoceros, C-dichaeta. Journal of Phycology 2008; 44: 152-163.

Belis CA, Pernigotti D, Pirovano G, Favez O, Jaffrezo JL, Kuenen J, et al. Evaluation of receptor and chemical transport models for PM10 source apportionment. Atmospheric Environment: X 2020; 5: 100053.

Bonazza A, Messina P, Sabbioni C, Grossi CM, Brimblecombe P. Mapping the impact of climate change on surface recession of carbonate buildings in Europe. Science of the Total Environment 2009; 407: 2039-2050.

Bonazza A, Sabbioni C, Ghedini N. Quantitative data on carbon fractions in interpretation of black crusts and soiling on European built heritage. Atmospheric Environment 2005; 39: 2607-2618.

Brimblecombe P, Grossi CM. Aesthetic thresholds and blackening of stone buildings. Science of the Total Environment 2005; 349: 175-189.

Calparsoro E, Maguregui M, Giakoumaki A, Morillas H, Madariaga JM. Evaluation of black crust formation and soiling process on historical buildings from the Bilbao metropolitan area (north of Spain) using SEM-EDS and Raman microscopy. Environmental Science and Pollution Research 2017; 24: 9468-9480.

Cesari D, Donateo A, Conte M, Contini D. Inter-comparison of source apportionment of PM10 using PMF and CMB in three sites nearby an industrial area in central Italy. Atmospheric Research 2016; 182: 282-293.

De Marco A, Screpanti A, Mircea M, Piersanti A, Proietti C, Fornasier MF. High resolution estimates of the corrosion risk for cultural heritage in Italy. Environmental Pollution 2017; 226: 260-267.

Di Turo F, Proietti C, Screpanti A, Fornasier MF, Cionni I, Favero G, et al. Impacts of air pollution on cultural heritage corrosion at European level: what has been achieved and what are the future scenarios. Environmental Pollution 2016; 218: 586-594.

Drinovec L, Mocnik G, Zotter P, Prevot ASH, Ruckstuhl C, Coz E, et al. The "dual-spot" Aethalometer: an improved measurement of aerosol black carbon with real-time loading compensation. Atmospheric Measurement Techniques 2015; 8: 1965-1979.

Fermo P, Goidanich S, Comite V, Toniolo L, Gulotta D. Study and characterization of environmental deposition on marble and surrogate substrates at a monumental heritage site. Geosciences 2018; 8.

Fermo P, Turrion RG, Rosa M, Omegna A. A new approach to assess the chemical composition of powder deposits damaging the stone surfaces of historical monuments. Environmental Science and Pollution Research 2015; 22: 6262-6270.

Giavarini C, Santarelli ML, Natalini R, Freddi F. A non-linear model of sulphation of porous stones: Numerical simulations and preliminary laboratory assessments. Journal of Cultural Heritage 2008; 9: 14-22.

Giussani B, Monticelli D, Rampazzi L. Role of laser ablation-inductively coupled plasma-mass spectrometry in cultural heritage research: A review. Analytica Chimica Acta 2009; 635: 6-21.

Ivančič M, Geregorič A, Lavrič G, Alföldy B, Ježek I, Hasheminassab S, et al. Two-year-long high-time-resolution apportionment of primary and secondary carbonaceous aerosols in the Los Angeles Basin using an advanced total carbon–black carbon (TC-BC(λ)) method. Science of the Total Environment 2022; 848: 157606.

Kušan AC, Kroflič A, Grgić I, Ciglenečki I, Frka S. Chemical characterization of fine aerosols in respect to water-soluble ions at the eastern Middle Adriatic coast. Environmental Science and Pollution Research 2020; 27: 10249-10264.

Laskin A, Laskin J, Nizkorodov SA. Chemistry of atmospheric brown carbon. Chemical Reviews 2015; 115: 4335-4382.

Lombardo T, Ionescu A, Chabas A, Lefevre RA, Ausset P, Candau Y. Dose-response function for the soiling of silica-soda-lime glass due to dry deposition. Science of the Total Environment 2010; 408: 976-984.

Manning MI, Martin RV, Hasenkopf C, Flasher J, Li C. Diurnal Patterns in Global Fine Particulate Matter Concentration. Environmental Science & Technology Letters 2018; 5: 687-691.

Mansour K, Decesari S, Bellacicco M, Marullo S, Santoleri R, Bonasoni P, et al. Particulate methanesulfonic acid over the central Mediterranean Sea: Source region identification and relationship with phytoplankton activity. Atmospheric Research 2020; 237: 104837.

Marszałek M, Skowroński A. Black "marble": The characteristic material in the baroque architecture of Cracow (Poland). In: Dan MB, Přikryl R, Török Á, editors. Materials, Technologies and Practice in Historic Heritage Structures. Springer Netherlands, Dordrecht, 2010, pp. 93-106.

Martinsson J, Sporre MK, Pedehontaa-Hiaa G, Azeem HA. On the Relationship of Biogenic Primary and Secondary Organic Aerosol Tracer Compounds on the Aethalometer Model Parameters. Aerosol and Air Quality Research 2020; 20: 2654-2668.

Ogrizek M, Jaćimović R, Šala M, Kroflič A. No more waste at the elemental analysis of airborne particulate matter on quartz fibre filters. Talanta 2021; 226: 122110.

Ogrizek M, Kroflic A, Sala M. Critical review on the development of analytical techniques for the elemental analysis of airborne particulate matter. Trends in Environmental Analytical Chemistry 2022; 33.

Ozga I, Ghedini N, Giosue C, Sabbioni C, Tittarelli F, Bonazza A. Assessment of air pollutant sources in the deposit on monuments by multivariate analysis. Science of the Total Environment 2014; 490: 776-784.

Paatero P, Eberly S, Brown SG, Norris GA. Methods for estimating uncertainty in factor analytic solutions. Atmospheric Measurement Techniques 2014; 7: 781-797.

Rigler M, Drinovec L, Lavric G, Vlachou A, Prevot ASH, Jaffrezo JL, et al. The new instrument using a TC-BC (total carbon-black carbon) method for the online measurement of carbonaceous aerosols. Atmospheric Measurement Techniques 2020; 13: 4333-4351.

Saiz-Jimenez C. Deposition of arborne organic pollutants on historic buildings. Atmospheric Environment Part B-Urban Atmosphere 1993; 27: 77-85.

Saraga D, Maggos T, Degrendele C, Klanova J, Horvat M, Kocman D, et al. Multi-city comparative PM2.5 source apportionment for fifteen sites in Europe: The ICARUS project. Science of the Total Environment 2021; 751.

Srivastava D, Favez O, Petit JE, Zhang Y, Sofowote UM, Hopke PK, et al. Speciation of organic fractions does matter for aerosol source apportionment. Part 3: Combining off-line and on-line measurements. Science of the Total Environment 2019; 690: 944-955.

Tidblad J, Kucera V, Ferm M, Kreislova K, Brüggerhoff S, Doytchinov S, et al. Effects of air pollution on materials and cultural heritage: ICP Materials celebrates 25 years of research. International Journal of Corrosion 2012; 2012: 496321.

Todd MC, Washington R, Martins JV, Dubovik O, Lizcano G, M'Bainayel S, et al. Mineral dust emission from the Bodele Depression, northern Chad, during BoDEx 2005. Journal of Geophysical Research-Atmospheres 2007; 112.

Vidović K, Hočevar S, Menart E, Drventić I, Grgić I, Kroflič A. Impact of air pollution on outdoor cultural heritage objects and decoding the role of particulate matter: a critical review. Environmental Science and Pollution Research 2022.

Wickham H. Reshaping data with the reshape package. Journal of Statistical Software 2007; 21: 1-20.

Wickham H, Averick M, Bryan J, Chang W, McGowan LDA, François R, et al. Welcome to the Tidyverse. Journal of Open Source Software 2019; 4: 1686.

Winkler A, Contardo T, Lapenta V, Sgamellotti A, Loppi S. Assessing the impact of vehicular particulate matter on cultural heritage by magnetic biomonitoring at Villa Farnesina in Rome, Italy. Science of the Total Environment 2022; 823.

For Table of Contents only.